Journal of Alloys and Compounds 509 (2011) 2789–2792

Contents lists available at ScienceDirect

Journal of Alloys and Compounds

journal homepage: www.elsevier.com/locate/jallcom

Structural, thermal and magnetic properties of Fe–Si–B–P–Cu melt-spun ribbons: Application of non-isothermal kinetics and the amorphous random anisotropy model

X.F. Miao, Y.G. Wang*, M. Guo

College of Materials Science and Technology, Nanjing University of Aeronautics and Astronautics, Nanjing 210016, China

ARTICLE INFO

Article history:
Received 16 July 2010
Received in revised form
15 November 2010
Accepted 15 November 2010
Available online 25 November 2010

Keywords:
Amorphous materials
Quenching
Kinetics
Thermal analysis

ABSTRACT

The microstructural variation of Fe–Si–B–P–Cu melt-spun ribbons was analyzed on the basis of non-isothermal kinetics and the amorphous random anisotropy model. The magnitude of latent heat of the crystallization process obtained from DSC curves increases with the increase of quenching wheel speed. The apparent activation energies of the nucleation and growth of α-Fe nanocrystallites increase as the quenching wheel speed increases. Thermal analysis implies that the size of the local short-medium order (cluster) in melt-spun ribbons reduces with the increase of quenching wheel speed. Meanwhile, magnetic measurements display that the coercivity of the stress-released ribbons decreases with the increasing quenching wheel speed. This confirms the thermal analysis results on the basis of the amorphous random anisotropy model. Combing thermal analysis with magnetic measurements, it is believed that the cluster size of the melt-spun ribbons decreases with the increase of the cooling rate during melt-spinning process. Nanocrystalline alloy with desirable microstructure and soft magnetic properties is anticipated to be obtained from an amorphous alloy prepared at an appropriate cooling rate by adjusting the quenching wheel speed.

1. Introduction

Nanocrystalline FeSiBCuP soft magnetic alloys are at the centre of intensive research due to their virtues of high B_S (~1.9 T), low core loss and free from expensive metal elements such as Nb, Zr, Mo, etc. [1]. Nanocrystalline soft magnetic alloys are usually prepared by the crystallization of melt-spun alloys. The microstructure of melt-spun alloys, which is believed to have a significant influence on the annealed nanocrystalline alloys, is worthy of researching and concerning. Based on the synchrotron X-ray diffraction and extended X-ray absorption fine structure measurements (EXAFS), molecular-dynamics and reverse Monte Carlo simulations manifest that amorphous alloy is efficiently packed by quasi-equivalent short-medium clusters [2–4]. However, direct observation of the detailed microstructure of amorphous alloy is still a challenge. As we all know melt spinning is a representative rapid-solidification technique, in which the heat of melt is instantaneously dissipated by a rotating copper wheel. A direct measurement of the cooling rate on the basis of thermoelectric technique proposed by Tkatch [5,6] shows that cooling rate increases with the quenching wheel speed. Variable cooling rates alter the diffusion process of atoms during the rapid solidification process and thus affect the degree of amorphicity [7] and local short-medium range order [8] in melt-spun ribbons. As a consequence, the thickness, microstructure and the microstructure-dependent properties of the melt-spun ribbons exhibit a strong dependence on quenching wheel speed [7–12].From the viewpoint of kinetics, the activation energies of the nucleation and growth of nanocrystallites, which determines the nanocrystallizaiton process and the microstructure of the annealed nanocrystalline alloy [13–17], are intimately related to the microstructure of the melt-spun alloys. Thermal analysis can give the activation energy of the crystallization process from the viewpoint of non-isothermal kinetics. In addition, for melt-spun alloys, the coercivity is a microstructure-dependent parameter making it as a useful probe to study the structural variations due to various quenching wheel speeds. In this work the influence of quenching wheel speed on the structural, thermal and magnetic properties of Fe–Si–B–P–Cu melt-spun ribbons was investigated and the microstructure variation of melt-spun ribbons was discussed on the basis of non-isothermal kinetics and the amorphous random anisotropy model.

2. Experimental

Alloy ingots with a nominal composition of $Fe_{81}Si_4B_{12}P_2Cu_1$ were prepared by arc melting under Ar (99.999%) atmosphere. The ingots were inverted and remelted four times to ensure homogeneity. Melt-spun ribbons were produced by a

* Corresponding author. Tel.: +86 25 52112901; fax: +86 25 52112626.
E-mail address: yingang.wang@nuaa.edu.cn (Y.G. Wang).

0925-8388/$ – see front matter © 2010 Elsevier B.V. All rights reserved.
doi:10.1016/j.jallcom.2010.11.101

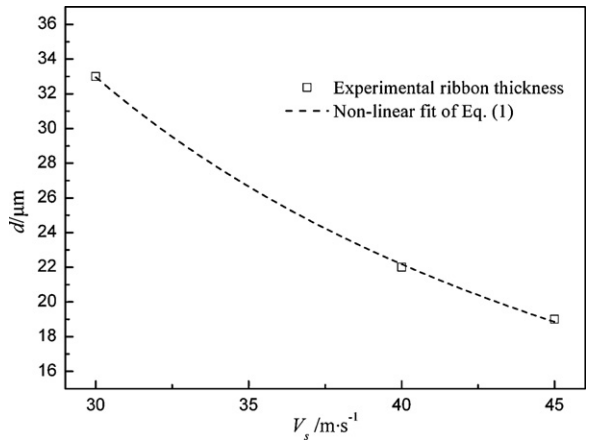

Fig. 1. Variations of the thickness d (open symbols) of $Fe_{81}Si_4B_{12}P_2Cu_1$ melt-spun ribbons versus quenching wheel speeds V_s. The dash line displays the non-linear fit of Eq. (1).

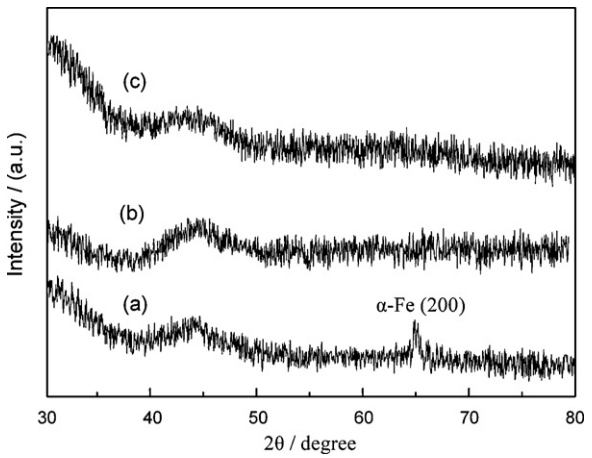

Fig. 2. XRD patterns of $Fe_{81}Si_4B_{12}P_2Cu_1$ melt-spun ribbons prepared at various quenching wheel speeds: (a) 30 m/s; (b) 40 m/s; (c) 45 m/s.

single-roller melt-spinning technique under Ar protective gas (99.999%) at various quenching wheel speeds of 30, 40, and 45 m/s, respectively. For all melt spinning experiments, the ejection temperature, gas ejection pressure, nozzle-wheel gap, crucible nozzle size and quantity of the used ingots were identical. All melt-spun ribbons were found to be completely ductile and in excellent surface quality.

The structural examinations of the melt-spun ribbons were carried out by X-ray diffractometer (XRD, Bruker D8) using Cu Kα_1 radiation. The thermal behavior of the melt-spun ribbons were measured with a differential scanning calorimeter (Diamond heat flux DSC, PerkinElmer) under a N_2 gas flow at heating rates of 20, 30, 40, 60 and 80 K/min, respectively. The temperature and enthalpy were calibrated using indium and zinc standards for all heating rates. The activation energies of the crystallization process for melt-spun ribbons were determined by non-isothermal crystallization kinetics. In order to release the internal stress during the melt spinning process, melt-spun ribbons were annealed at a temperature below crystallization temperatures in a flowing Ar atmosphere. The magnitudes of the coercivity of melt-spun ribbons were measured by a DC B–H loop tracer.

3. Results and discussion

3.1. Structural analysis

According to solidification kinetics [18,19], an empirical relationship between the quenching wheel speed V_s and the melt-spun ribbon thickness d was proposed:

$$d \propto \frac{1}{V_s^m} \quad (1)$$

where m is a parameter reflecting the degree of the ribbon thickness dependence on quenching wheel speed.

Fig. 1 shows the ribbon thickness d as a function of quenching wheel speed V_s (open symbols). The parameter m with a value of 1.38, obtained by the non-linear fit of Eq. (1) to the experimental data, is larger than that reported in other literatures [7,9]. This indicates a strong dependence of quenching wheel speed on the ribbon thickness for the present alloy system, which may result from the high contents of metal element (Fe: 81 at.%). Metal elements usually have a higher thermal conductivity than metalloid elements and are more sensitive to the heat transfer during the quenching process. As a consequence, the present alloy system displays a strong dependence of ribbon thickness on quenching wheel speed.

The XRD patterns of $Fe_{81}Si_4B_{12}P_2Cu_1$ melt-spun ribbons at various quenching wheel speeds are demonstrated in Fig. 2. Only a broad peak at around $2\theta = 45^\circ$ exhibiting an amorphous character was detected for the ribbons prepared at the quenching wheel speeds of 40 and 45 m/s, while a noticeable diffraction peak revealing a partial nanocrystallization appeared at around $2\theta = 65^\circ$ corresponding to α-Fe (2 0 0) for the ribbon at a wheel speed of 30 m/s. During the rapidly quenching process of melt, crystallization is a competing process with amorphization and is related to atomic diffusion. Higher wheel speed brings about a larger cooling rate which restrains the atomic diffusion and depresses crystallization process. As a result, it is favorable to obtain amorphous ribbons at high quenching wheel speeds, which is in accordance to previous reports [7]. On the other hand, the variation in atomic diffusion caused by various wheel speeds probably leads to different microstructures for amorphous phases, however, which cannot be detected by XRD measurements. For this reason, thermal and magnetic measurements are employed for a further analysis on the microstructure of melt-spun ribbons.

3.2. Thermal analysis

Fig. 3 presents DSC curves measured at a heating rate of 20 K/min for $Fe_{81}Si_4B_{12}P_2Cu_1$ alloys quenched at wheel speeds of 30, 40, and 45 m/s, respectively. Obviously the crystallization occurs in two distinct stages corresponding to the nanocrystallization process of α-Fe and formation of Fe–B compounds [20], respectively. DSC curves measured at heating rates of 30, 40, 60 and 80 K/min exhibit a similar crystallization behavior (not shown). The characteristic temperatures of the first exothermic peak in all DSC curves are listed in Table 1. The area of exothermic peak in DSC curve is proportional to the latent heat of crystallization which reflects the degree of amorphicity of melt-spun ribbons [7,21]. For melt-spun alloys with an identical composition, higher latent heat during crys-

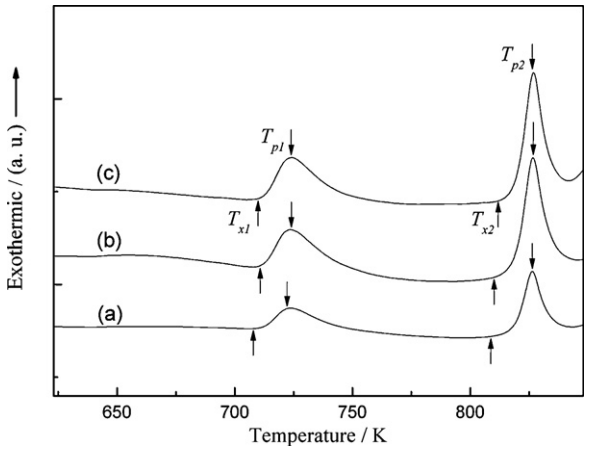

Fig. 3. DSC curves at a heating rate of 20 K/min for $Fe_{81}Si_4B_{12}P_2Cu_1$ melt-spun ribbons quenched at various wheel speeds: (a) 30 m/s; (b) 40 m/s; (c) 45 m/s.

Table 1
The characteristic temperatures T_{x1} and T_{p1} obtained from DSC curves at various heating rates β for $Fe_{81}Si_4B_{12}P_2Cu_1$ melt-spun ribbons quenched at different wheel speeds V_s.

V_s (m/s)	β (K/min)	T_{x1} (K) (±1)	T_{p1} (K) (±1)
30	20	703	724
	30	707	730
	40	712	735
	60	718	744
	80	724	752
40	20	707	726
	30	711	732
	40	716	738
	60	722	746
	80	727	753
45	20	708	727
	30	713	734
	40	717	739
	60	723	747
	80	728	754

tallization process demonstrates a higher degree of amorphicity. As determined from Fig. 3, the magnitudes of latent heat of the crystallization process are 43.3, 70.5, 71.9 J/g, for the melt-spun ribbons quenched at the wheel speed of 30, 40, 45 m/s, respectively. This result implies that the degree of amorphicity increases with quenching wheel speed, which is in agreement with the XRD measurements as well as other reports [7]. The rather small magnitude of latent heat for the melt-spun ribbon quenched at a speed of 30 m/s is due to the partially crystallized nanocrystallites as shown in XRD measurements (Fig. 2(a)).

The onset (T_{x1}) and peak (T_{p1}) crystallization temperatures of the first exothermic peak are associated with the nucleation and growth processes of α-Fe nanocrystallites, respectively [13,22,23]. The apparent activation energies of the nucleation (E_{x1}) and growth (E_{p1}) processes for melt-spun alloys can be calculated by the Kissinger's equation [24]:

$$\ln\left(\frac{T^2}{\beta}\right) = \ln\left(\frac{E_a}{R}\right) - \ln\nu + \frac{E_a}{RT} \quad (2)$$

where β is the heating rate, E_a is the apparent activation energy (E_{x1} for nucleation or E_{p1} for growth), ν is the frequency factor, R is gas constant, T is the characteristic temperature as listed in Table 1 (T_{x1} for nucleation or T_{p1} for growth). The $\ln T^2/\beta$ versus 10^3T^{-1} for the melt-spun ribbons prepared at various quenching wheel speeds are plotted in Fig. 4(a) and (b) for nucleation and growth processes, respectively. A straight line can be fitted with the slope of E_a/R, which can deduce the apparent activation energy E_a. As shown in Fig. 4(a) and (b), the activation energies of both nucleation E_{x1} and growth E_{p1} of α-Fe nanocrystallites for the present alloy system are similar to that of the previous report [13]. Fig. 5 reveals the dependence E_{x1} and E_{p1} on quenching wheel speed for $Fe_{81}Si_4B_{12}P_2Cu_1$ melt-spun ribbons. Obviously both E_{x1} and E_{p1} show an evident increasing tendency with the quenching wheel speed, i.e., the crystallization becomes harder for the melt-spun ribbons quenched at higher wheel speeds. It is well known that the crystallization process has an intimate relation with the microstructure of the melt-spun ribbon. Crystal-like clusters (local short-medium range order), formed in the melt-spun ribbons owing to the chemical interaction among the constituent elements, has been confirmed by EXAFS measurements and reverse Monte Carlo simulations [3,4]. As for the present Fe–Si–B–P–Cu alloys system, (Cu, P)-rich clusters in melt-spun alloys have been proposed to act as the heterogeneous nucleation sites for α-Fe nanocrystallites during the nanocrystalline process [1,13]. Besides, the size and number density of the clusters have a significant influence on the crystallization process

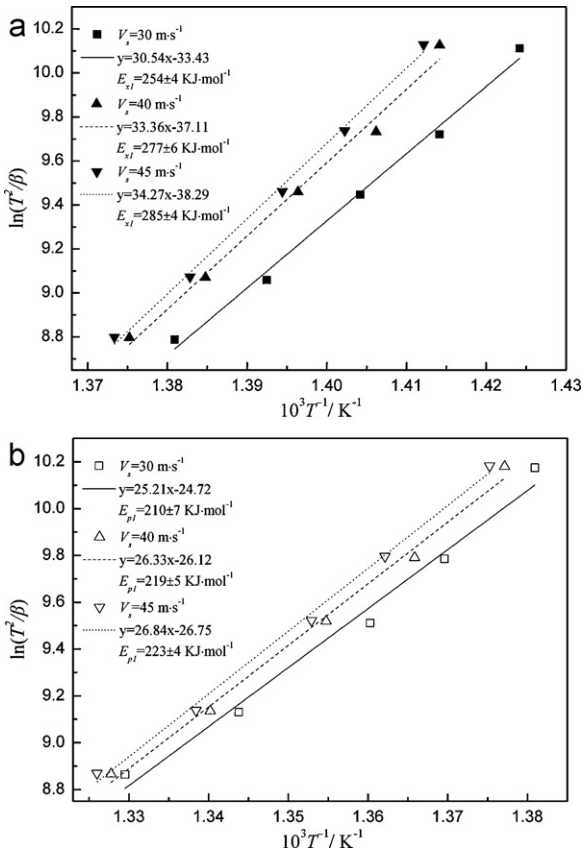

Fig. 4. Kissinger plots for the onset temperature T_{x1} (a) and peak temperature T_{p1} (b) of crystallization for $Fe_{81}Si_4B_{12}P_2Cu_1$ melt-spun ribbons.

of the melt-spun ribbons. Only can the crystal-like clusters with a size larger than a critical size (4∼6 nm) serve as the nucleation sites for α-Fe nanocrystallites [20]. The larger E_{x1} values obtained at higher quenching wheel speeds suggest a smaller size and lower number density of clusters, which are unfavorable for the nucleation process. In addition, taking into account the factor of atomic diffusion during the growth of nanocrystallites, the higher E_{p1} for the melt-spun ribbons prepared at higher wheel speeds implies a more uniform distribution of atoms. As a consequence, one can conclude that the size and number density of the local short-medium order (cluster) decrease as the quenching wheel speed increases.

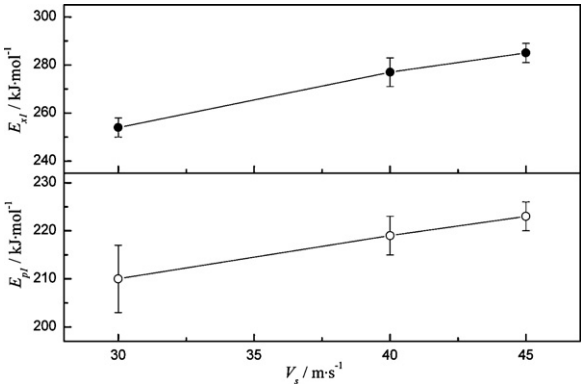

Fig. 5. Dependence of apparent activation energies of nucleation (E_{x1}) and growth (E_{p1}) processes on the quenching wheel speed for $Fe_{81}Si_4B_{12}P_2Cu_1$ melt-spun ribbons. The lines are guides for the eye.

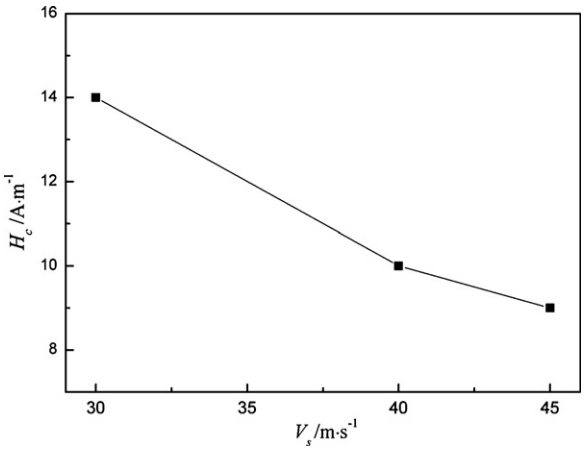

Fig. 6. . Coercivity of $Fe_{81}Si_4B_{12}P_2Cu_1$ ribbons annealed at 623 K for 10 min as a function of the quenching wheel speed. The line is a guide for the eye.

3.3. Magnetic properties

All melt-spun ribbons were annealed at 623 K (below crystallization temperatures ~710 K) for 10 min before magnetic measurements to release the internal stress during the melt spinning process. Fig. 6 exhibits the quenching wheel speed dependence of coercivity for the annealed ribbons. One can see that coercivity decreases from 14 A/m to 9 A/m as the quenching wheel speed increases from 30 m/s to 45 m/s.

The magnetic properties of amorphous ribbons depend on the random anisotropy caused by local short-medium order [25] as well as the stress-induced anisotropy [26]. The internal stress in the amorphous ribbons increases with the quenching wheel speed due to the increasing cooling rate, which will give rise to the deterioration of soft magnetic properties [27]. However, this is incompatible with the present experimental results, i.e. soft magnetic properties improve with increasing wheel speeds. This implies that little internal stress remained after the annealing treatment below crystallization temperatures and the stress-induced anisotropy takes a minor effect on the soft magnetic properties for the annealed amorphous ribbons. Therefore, one can believe that the short-medium clusters play a determinant role in soft magnetic properties of the present amorphous alloys.

According to the amorphous random anisotropy model proposed by Alben et al [25]:

$$H_c \propto \frac{K^4 d^6}{A^3 M} \tag{3}$$

where H_c denotes the coercivity, K denotes the local uniaxial anisotropy, d denotes the local short-medium range ordering length (i.e. cluster size), A represents the magnetic exchange correlation stiffness, M represents the magnetization. The coercivity (H_c) is very sensitive to the cluster size (d) showing a sixth power dependence. The cluster size of the amorphous ribbon decreases with the increase of the quenching wheel speed. As a result, a decrease of coercivity with the increase of quenching wheel speed is predicted by the amorphous random anisotropy model, which is well confirmed by the magnetic measurements, as shown in Fig. 6. Smaller size of local short-medium cluster owing to higher quenching wheel speeds, leads to a lower random anisotropy and eventually superior soft magnetic properties.

Additionally, the coercivity of the partially crystallized ribbon quenched at a wheel speed of 30 m/s is markedly larger than that of the other amorphous ribbons quenched at higher wheel speeds. This may partially originate from the fact that with respect to the amorphous matrix the crystallized nanocrystallites show large magnetocrystalline anisotropy which cannot be averaged out by the magnetic exchange coupling between nanocrystallites [26,28].

Combing thermal analysis with magnetic measurements, one can conclude that the cluster size of the melt-spun ribbons decreases with the increase of quenching wheel speed. Besides, Tkatch [5,6] proposed that cooling rate during the melt-spinning process increases with the quenching wheel speed. Therefore, the cluster size of the melt-spun ribbon is believed to reduce with the increase of cooling rate during melt-spinning process.

4. Conclusions

The structural, thermal and magnetic properties of Fe–Si–B–P–Cu melt-spun ribbons were investigated and the variation of microstructure of amorphous ribbons was discussed on the basis of non-isothermal kinetics and the amorphous random anisotropy model. The magnitudes of latent heat of the crystallization process increase with the increase of the quenching wheel speed, indicating a higher degree of amorphicity at higher wheel speeds. The increase of activation energies for both nucleation and growth processes implies that the size and number density of the local short-medium order (cluster) decrease as the quenching wheel speed increases. Besides, the decrease in coercivity with the increase of quenching wheel speed verifies the reduction of cluster size based on the amorphous random anisotropy model. It is found that the cluster size of the melt-spun ribbons decreases with the increase of the cooling rate during melt-spinning process. The desirable microstructure and soft magnetic properties of annealed nanocrystalline alloys are expected to be obtained from an amorphous alloy prepared at an appropriate cooling rate by adjusting the quenching wheel speed.

References

[1] A. Makino, H. Men, T. Kubota, K. Yubuta, A. Inoue, Mater. Trans., JIM 50 (2009) 204.
[2] F. Saporiti, M. Boudard, F. Audebert, J. Alloys Compd. 495 (2010) 309.
[3] H.W. Sheng, W.K. Luo, F.M. Alamgir, J.M. Bai, E. Ma, Nature 439 (2006) 419.
[4] Y.Q. Cheng, H.W. Sheng, E. Ma, Phys. Rev. B 78 (2008) 014207.
[5] V.I. Tkatch, A.I. Limanovskii, S.N. Denisenko, S.G. Rassolov, Mater. Sci. Eng. A 323 (2002) 91.
[6] V.I. Tkatch, S.N. Denisenko, O.N. Beloshov, Acta Mater. 45 (1997) 2821.
[7] F. Shahri, A. Beitollahi, J. Non-Cryst. Solids 354 (2008) 1487.
[8] L. Zhang, Y.S. Wu, X.F. Bian, H. Li, W.M. Wang, S. Wu, J. Non-Cryst. Solids 262 (2000) 169.
[9] H. Fiedler, H. Muhlbach, G. Stephani, J. Mater. Sci. 19 (1984) 3229.
[10] H. Lefaix, P. Vermaut, D. Janickovic, P. Svec, R. Portier, F. Prima, J. Alloys Compd. 483 (2009) 168.
[11] J.B. Sun, Z.X. Zhang, C.X. Cui, W. Yang, P. Guo, D. Han, B.L. Wang, J. Alloys Compd. 476 (2009) 575.
[12] S. Aich, J.E. Shield, J. Alloys Compd. 502 (2010) 63.
[13] L.Y. Cui, H. Men, S. Makino, T. Kubota, K. Yubuta, M. Qi, A. Inoue, Mater. Trans., JIM 50 (2009) 2515.
[14] D.M. Minic, A. Gavrilovic, P. Angerer, D.G. Minic, A. Maricic, J. Alloys Compd. 482 (2009) 502.
[15] H.T. Zhou, Z.K. Zhao, X. Zhou, B. Yan, J.W. Zhong, Q.B. Li, J. Alloys Compd. 475 (2009) 706.
[16] Y. Xu, X. Huang, A.G. Ramirez, J. Alloys Compd. 480 (2009) L13.
[17] F. Sun, T. Gloriant, J. Alloys Compd. 477 (2009) 133.
[18] R.C. Rahl, Mater. Sci. Eng. 1 (1967) 313.
[19] P.H. Shingu, R. Ozaki, Met. Trans. A 6A (1995) 33.
[20] Y.M. Chen, T. Ohkubo, M. Ohta, Y. Yoshizawa, K. Hono, Acta Mater. 57 (2009) 4463.
[21] M. Ohta, Y. Yoshizawa, J. Magn. Magn. Mater. 321 (2009) 2220.
[22] F.X. Qin, H.F. Zhang, B.Z. Ding, Z.Q. Hu, Intermetallics 12 (2004) 1197.
[23] Y.D. Sun, Z.Q. Li, J.S. Liu, J.N. Yang, M.Q. Cong, J. Alloys Compd. 506 (2010) 302.
[24] H.E. Kissinger, Anal. Chem. 29 (1957) 1702.
[25] R. Alben, J.J. Becker, M.C. Chi, J. Appl. Phys. 49 (1978) 1653.
[26] A. Hernando, M. Vazquez, T. Kulik, C. Prados, Phys. Rev. B 51 (1995) 3581.
[27] T. Kulik, M. Kopcewicz, J. Magn. Magn. Mater. 215–216 (2000) 455.
[28] M. Ohta, Y. Yoshizawa, Appl. Phys. Lett. 91 (2007) 062517.